

Steric-Hindrance-Driven Shape Transition in PbS Quantum Dots: Understanding Size-Dependent Stability

Hyekyoung Choi,^{†,‡,⊥} Jae-Hyeon Ko,^{§,⊥} Yong-Hyun Kim,^{*,§} and Sohee Jeong^{*,†,‡}

[†]Nanomechanical Systems Research Division, Korea Institute of Machinery and Materials, Daejeon 305-343, Republic of Korea

[‡]Department of Nanomechatronics, University of Science and Technology, Daejeon 305-350, Republic of Korea

[§]Graduate School of Nanoscience and Technology (WCU), KAIST, Daejeon 305-701, Republic of Korea

Supporting Information

ABSTRACT: Ambient stability of colloidal nanocrystal quantum dots (QDs) is imperative for low-cost, high-efficiency QD photovoltaics. We synthesized air-stable, ultrasmall PbS QDs with diameter (D) down to 1.5 nm, and found an abrupt transition at $D \approx 4$ nm in the air stability as the QD size was varied from 1.5 to 7.5 nm. X-ray photoemission spectroscopy measurements and density functional theory calculations reveal that the stability transition is closely associated with the shape transition of oleate-capped QDs from octahedron to cuboctahedron, driven by steric hindrance and thus size-dependent surface energy of oleate-passivated Pb-rich QD facets. This microscopic understanding of the surface chemistry on ultrasmall QDs, up to a few nanometers, should be very useful for precisely and accurately controlling physicochemical properties of colloidal QDs such as doping polarity, carrier mobility, air stability, and hot-carrier dynamics for solar cell applications.

Lead chalcogenide (PbX, where X = S, Se) quantum dots (QDs) have been extensively investigated lately with a hope for realizing next-generation (low-cost, high-efficiency) photovoltaics.¹ In addition to their abundance, the large exciton Bohr radii of PbX could provide strong quantum confinement effects for colloidal QDs. This band gap tunability from infrared to ultraviolet could enable a multi-junction solar cell absorbing the entire solar spectrum. Furthermore, successful utilization of high-energy photons above band gaps could promise a single-junction solar energy conversion efficiency over the Shockley–Queisser limit, 33%.² Despite these advantages as light-absorbing materials for next-generation solar cells, a working QD-based device has long been a challenge because of uncontrolled surface defects and thus degradation of QDs during post-processing for device fabrication and, more seriously, during solar cell operation. Recent advances in surface passivation engineering resulted in a noticeable photoconversion efficiency of >7%.³ Urgently demanded is a breakthrough in improving material and device stability in atmospheric ambient condition. It is known that, in air, PbSe QDs undergo critical surface oxidation,⁴ but PbS QDs are somewhat resistant to surface corrosion.⁵ However, even basic microscopic information about colloidal PbX QDs such as surface geometry, ligand passivation, and nanocrystal shape is vastly lacking, and thus the air stability issue is not yet totally solved.

In this Communication, we report the synthesis of air-stable, ultrasmall PbS QDs and propose an oleate-passivated Pb-rich (111)-only surface chemistry of octahedral PbS QDs on the basis of X-ray photoemission spectroscopy (XPS) measurements and density functional theory (DFT) calculations. We have found that the air stability of QDs undergoes a sharp transition when the QD size is ~ 4 nm. The measured Pb/S ratio and the calculated surface energy of the oleate-passivated Pb-rich (111) surface indicate that a shape transition from (111)-only octahedron to (111)/(100) cuboctahedron should occur as QD size increases, driven by the increased steric hindrance among the capping groups for large QDs. The size-dependent air stability is thus attributed to the (111)-to-(100) transition of QD facets, i.e., from the air-stable ligand-passivated (111) facets to the bare self-passivated (100) facets that are prone to surface oxidation in ambient conditions.

The band gap of PbS QDs can be tuned by changing the nanocrystal size. A synthetic route for creating size-tuned PbS QDs in the diameter (D) range of 2.6–7.2 nm, corresponding to absorption peak ($1S_{\max}$) of 825–1750 nm and band gap of 0.7–1.5 eV, was well established⁶ and widely adapted for recent photovoltaic device fabrications. By reducing reactive Pb precursors, one could obtain PbS QDs as small as $D = 2.6$ nm.^{6a} Smaller QDs <2.6 nm could provide larger band gaps, offering improved open-circuit voltage in QD-based Schottky devices⁷ or QD-based quantum junction devices.⁸ Synthesis of ultrasmall PbS QDs <2.6 nm is not well established and is very challenging because of the highly reactive surfaces of ultrasmall QDs, which typically grow fast. In this work, we synthesized PbS QDs as small as 1.5 nm with an absorption peak of 480 nm, which are the smallest PbS QDs ever reported. Briefly, Pb(oleate)₂ in octadecene was reacted with the S precursor, bis(trimethylsilyl)sulfide, at 90 °C and cooled rapidly with hexane and ice-bath to stop fast crystal growth. Size-controlled QDs were then grown under relatively low growth temperatures of 5–50 °C (see SI for details). Unreacted precursors were removed by precipitation, and PbS QDs were redispersed in hexane or tetrachloroethylene for further characterization.

Figure 1A shows the absorption and photoluminescence (PL) spectra of ultrasmall PbS QDs, of which PL peaks at 680 nm with a Stokes shift of 200 nm. A high-resolution transmission electron microscopy (TEM) image is shown in Figure 1B. Based on the

Received: January 28, 2013

Published: March 15, 2013

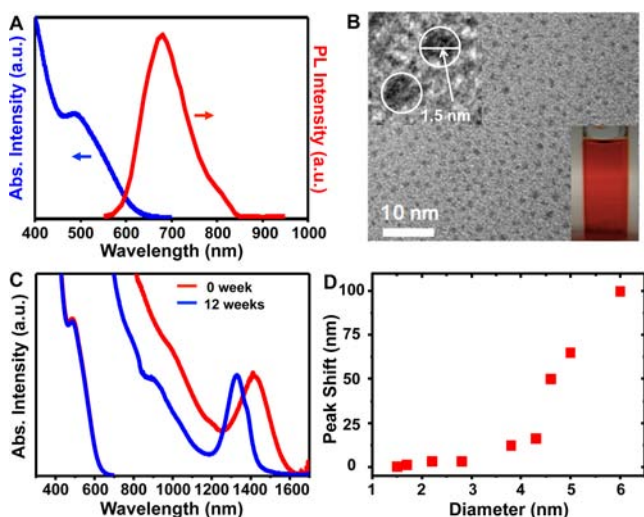


Figure 1. (A) Absorption and photoluminescence spectra of ultrasmall PbS QDs dispersed in tetrachloroethylene. (B) TEM image of the ultrasmall PbS QDs with $1S_{\max} = 480$ nm. (Inset) High-resolution TEM image of individual ultrasmall QDs showing $D \approx 1.5$ nm, and a photograph of a colloidal solution of ultrasmall QDs showing its daylight color is red. (C) Absorption spectra of ultrasmall and large QDs just after synthesis and after 12 weeks of being stored in ambient atmosphere, showing a blue peak shift. (D) Peak shift depending on QD size, showing a transition at ~ 4 nm.

image (inset), the QD size is estimated to be 1.5 nm. Because ultrasmall QDs absorb green and blue light, the QD-dispersed solution was red (Figure 1B inset). We further tuned the size of PbS QDs and obtained the absorption spectra with the excitonic transition ($1S_{\max}$) varying from 480 to 1640 nm (see SI for detailed synthesis and Figures S1 and S2).

Size-dependent air stability of PbS QDs was quantified by measuring the absorption spectra of QD-dispersed solutions stored in atmospheric ambient conditions for 12 weeks (see Figure 1C, Figure S3, and Table S1). The absorption edge was characteristically blue-shifted after 12 weeks. Large PbS QDs with $D = 6.1$ nm showed a 94 nm blue shift of $1S_{\max}$. At the other extreme, ultrasmall QDs did not show any noticeable peak shift, indicating that they are very stable in air. The $1S_{\max}$ peak shift was plotted as a function of QD diameter in Figure 1D. From the analysis, one can clearly notice a transition at ~ 4 nm, indicating that the air stability of PbS QDs is very size-dependent and critically varied at ~ 4 nm. The size-dependent air stability was also confirmed by monitoring the PL intensity (see Figure S4), which is a sensitive measure of surface degradation.⁹

The blue shifts of absorption peaks of PbS QDs can be attributed to surface oxidation under aerobic conditions. The poor air stability of PbSe QDs has been discussed in terms of surface oxidation. It was proposed that PbSe QDs undergo structural transformations in air by forming PbO, SeO₂, and PbSeO₃ at the surface within a few hours. Surface oxidation leads to uncontrolled size reduction (blue shift) and defect distribution, thereby deteriorating optical and electrical properties of the QDs.⁴ PbS QDs have been known to be more stable in air than PbSe, because S is more electronegative than Se. Also, it is known that the size-dependent air stability of PbS is very subjective to synthetic conditions.¹⁰ For example, oleate-capped, rather large PbS QDs with absorption peaks at 930 and 1500 nm showed noticeable degradation in air, but with rather high air stability for the smaller size,^{5b} consistent with our observation.

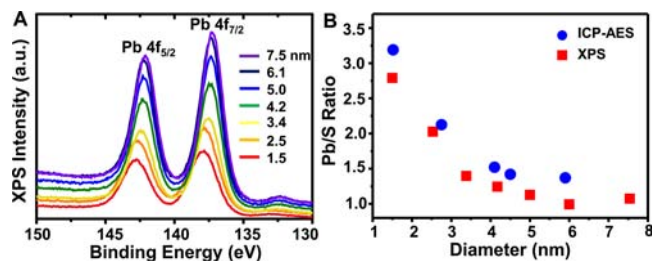


Figure 2. (A) High-resolution Pb 4f XPS spectra of PbS QDs with $D = 1.5$ – 7.5 nm. (B) Diameter-dependent Pb/S atomic ratio of PbS QDs obtained from ICP-AES and XPS.

When synthesized from PbCl₂, PbS QDs with an absorption peak at 1590 nm showed remarkable air stability compared to similar-size oleate-capped PbS QDs, probably because of additional passivation by chlorides.⁵ The air stability of ultrasmall, oleate-capped PbS QDs and the stability transition at ~ 4 nm, uniquely observed in our experiment, can thus be important missing links for understanding the surface chemistry of PbS QDs.

XPS is a viable tool for chemical analysis of nanostructured materials and has been widely used for chemical state identification of PbX QDs.¹⁰ To understand the size-dependent ambient stability, we performed XPS studies of air-free PbS QD films with diameters ranging from 1.5 to 7.5 nm (see SI, Figure 2, Figures S5 and S6, and Tables S2 and S3 for details). XPS spectra in the range 130–150 eV are dominated by two features from Pb 4f_{5/2} and Pb 4f_{7/2}, as indicated in Figure 2A. As the QD size decreases, the Pb 4f core levels shift toward high binding energy, representing that Pb atoms in smaller QDs are more oxidized, or positively ionized on average. In colloidal PbS QDs, there could exist two kinds of Pb²⁺ chemical states: one is the bulk Pb²⁺ cation surrounded mostly with S²⁻ anions, and the other is the surface Pb²⁺ cation surrounded partly by COO⁻ anions from oleate. By deconvoluting the measured XPS spectra with two chemical states of Pb–S (bulk) and Pb–O (bulk), we can estimate the $Pb_{\text{surface}}/Pb_{\text{bulk}}$ ratios (Table S3) as 4.7 for ultrasmall QDs and 0.6 for large-size QDs.

More accurate chemical analysis of PbS QDs can be done by estimating the Pb/S atomic ratio from integration of Pb 4f and S 2s XPS peaks (Table S2). Estimated atomic ratios confirm that PbS QDs are all Pb-rich regardless of size. Noticeably, the ultrasmall QDs have a Pb/S ratio close to 3, and the ratio quickly drops as QD size increases. We also performed elemental analysis using inductively coupled plasma atomic emission spectrometry (ICP-AES), showing a good correlation with the XPS result (Figure 2B).

It has been proposed that PbS QDs in the rock-salt structure can be faceted with the nonpolar (100) and polar (111) surfaces,¹¹ depending on QD size, capping ligand, and coverage. Our XPS elemental analysis revealed that, for the ultrasmall PbS QDs, Pb²⁺ is in the most ionized state supported by the highest XPS binding energy, and the Pb/S ratio approaches 3. The extreme Pb-rich condition indicates that the ultrasmall PbS QDs must be mostly covered with the Pb-terminated (111) surface. In our synthetic conditions, Pb and S were supplied in the forms of Pb(oleate)₂ and bis(trimethylsilyl)sulfide. Because the bis(trimethylsilyl) compound is highly volatile, leaving S behind, oleate-passivated Pb-rich (111) surfaces should dominate during the synthesis. The Pb atom in the Pb-terminated, unpassivated (111) surface is half-coordinated (three neighboring S atoms), compared to the bulk rock-salt form (six neighboring S atoms), thus being in the Pb⁺ state. To be in the Pb²⁺ state and thus in

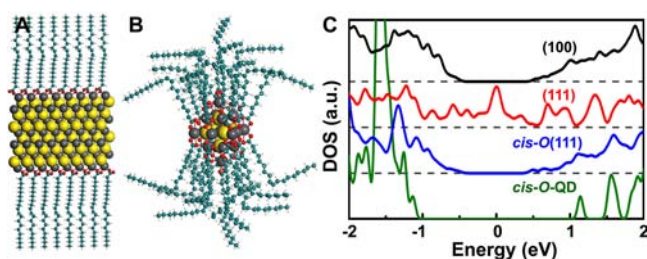


Figure 3. Ball-and-stick models of Pb-rich *cis*-O(111)-terminated (A) surface and (B) ultrasmall QDs (gray, Pb; yellow, S; red, O; cyan, C; white, H). (C) Calculated electronic DOSs of (100), (111), *cis*-O(111), and *cis*-O QDs near the Fermi energy ($E = 0$).

Table 1. DFT Surface Energy (γ , J/m²) of Various PbS Surface Systems (See Figure S7)^a

	(100)	(111)	F(111)	A(111)	N(111)	<i>trans</i> -O(111)	<i>cis</i> -O(111)
γ	0.22	1.04	-0.29	-0.05	0.8	1.12	1.92

^a(100) and (111) represent bare stoichiometric surfaces. L(111) represents L-capped Pb-rich (111) surface passivated with formate (F), acetate (A), nonanoate (N), *trans*-oleate (*trans*-O), or *cis*-oleate (*cis*-O).

perfect passivation, one more electron of Pb should be coordinated with a monovalent anion such as oleate. So, every exposed Pb ion in the flat (111) surface should be exactly coordinated with one anionic ligand for perfect passivation, as named L(111) hereafter.

When forming nanocrystal PbS QDs, the surface energy of the oleate-capped, Pb-rich (111) surface should compete with the surface energy of the nonpolar, self-passivated (100) surface. To see the competition mechanics,¹² we calculated, based on the DFT formulation, surface energies of (100), (111), and Pb-rich ligand-capped L(111) passivated with formate (F), acetate (A), nonanoate (N), *trans*-oleate (*trans*-O), and *cis*-oleate (*cis*-O). We also calculated surface energies of formate-, acetate-, and *cis*-oleate-capped ultrasmall PbS QDs (see Figures 3 and S7). The theoretical surface energy γ was defined as¹³

$$\gamma = [E(n\text{PbS}/m\text{PbL}_2) - nE(\text{PbS}) - mE(\text{PbL}_2)]/A \quad (1)$$

where E is DFT total energy, A is surface area, n and m represent respectively the numbers of PbS and PbL₂ units in the system, and L represents the capping ligand. The total energies of PbS and PbL₂ were taken respectively from bulk PbS and PbL₂ precursor molecules. The obtained surface energy is summarized in Table 1.

The nonpolar (100) surface is self-passivated without any dangling bond or reactive electron at the Fermi energy, as represented by semiconducting density of states (DOS) with a band gap of 1 eV (Figure 3C). In contrast, the polar (111) surface is not electronically passivated, showing metallic DOS with many surface states near the Fermi energy. Because of this, the surface energy (0.22 J/m²) of the self-passivated, nonpolar (100) surface is much smaller than that (1.04 J/m²) of the unpassivated, polar (111) surface, consistent with previously reported results.¹⁴ The calculated (100) surface energy of PbS is comparable to that of NaCl, i.e., 0.14–0.24 J/m² from DFT and 0.18–0.38 J/m² from experiment.¹⁵ So, cubic PbS consisting of all (100) facets is most likely to form when no passivating ligand presents.

When the (111) surface is passivated with PbL₂ ligand groups to form a Pb-rich L(111) surface, complete surface passivation is

observed in the electronic DOS with band gaps, as clearly seen in Figure S7c–f. Perfect passivation is guaranteed because every surface Pb in the Pb-rich L(111) surface is coordinated with one ligand molecule L. The calculated surface energy of L(111) ranges from -0.29 to 1.92 J/m², depending on the size and type of ligand molecules (Table 1). Remarkably, the F(111) and A(111) surfaces have much lower surface energies than the (100) has. This means that formate- and acetate-capped PbS nanocrystals, according to the Wulff construction,^{11c} will favor the octahedral shape consisting of all L(111). On the other hand, the surface energies of nonanoate- and oleate-capped (111) are greater than that of (100), even if reactive surface states are completely passivated (Figure S7). The high surface energy could thus be attributed to the steric hindrance among ligand molecules rather tightly jammed on the L(111) surface. The *cis*-oleate generates the strongest ligand–ligand repulsion or steric hindrance between molecules, resulting in a surface energy of 1.92 J/m². Therefore, steric hindrance can determine the shape of nanocrystal QDs.

The extreme Pb/S ratio (~3) of ultrasmall PbS QDs can only be explained with a nanocrystal QD model entirely covered with the *cis*-O(111), but this idea, at first glance, contradicts the highest calculated surface energy of *cis*-O(111). We postulate that the surface energy of *cis*-O(111) is dependent on the size of the QDs because the steric hindrance can be mitigated at nanoscale QD geometry. Indeed, our direct DFT calculations of eq 1 show that formate-, acetate-, and *cis*-oleate-capped ultrasmall octahedral QDs, consisting of 19 Pb atoms, 6 S atoms, and 26 ligand molecules (up to 1403 atoms), have similar surface energies of -0.19, -0.18, and -0.13 J/m², respectively, rather independent of the ligand size. This is clearly in contrast to the surface energies of the flat surface models. The ultrasmall L-QD models are all semiconducting, with a band gap of 2.2 eV, as shown in Figures 3 and S7. DFT-optimized geometries, shown in Figure 3A,B, clearly indicate that the steric hindrance of the flat *cis*-O(111) surface is significantly relaxed on the curved nanostructured *cis*-O QD.

Therefore, Pb-rich ultrasmall PbS QDs should be octahedral and covered with *cis*-O(111). As QD size increases, the surface energy of the *cis*-oleate-capped octahedral QDs increases, converging to the value of the flat *cis*-O(111) surface. When the *cis*-O(111) surface energy of QDs is comparable to the (100) surface energy for a certain size of QDs, the (100) facet should appear, truncating the octahedron and thus leading to a shape transition to cuboctahedron. The appearance of the stoichiometric (100) surface is another source of the Pb/S ratio reduction for large QDs, in addition to the reduced surface-to-bulk ratio.

With this in mind, we reconstructed size-dependent shapes of oleate-capped Pb-rich PbS QDs based on the measured Pb/S ratio. We first traced all possible Pb/S ratios of octahedral and cuboctahedral QDs depending on particle size, as marked with background symbols in Figure 4. Because there is some uncertainty in estimating the QD size in both experiment and theory, we used the farthest Pb–Pb distance in theory. For ultrasmall QDs with $D < 3$ nm, the measured Pb/S ratios well correspond to those of *cis*-O(111)-only octahedral QDs. For QDs > 3 nm in size, the measured Pb/S ratios are noticeably and consistently smaller than those of *cis*-O(111)-only QDs. The reduced Pb/S ratio can thus be explained by the truncation of octahedral QDs with the appearance of the stoichiometric (100) surface. Figure 4 inset illustrates the proposed QD models with the octahedral and cuboctahedral shapes as a function of QD size.

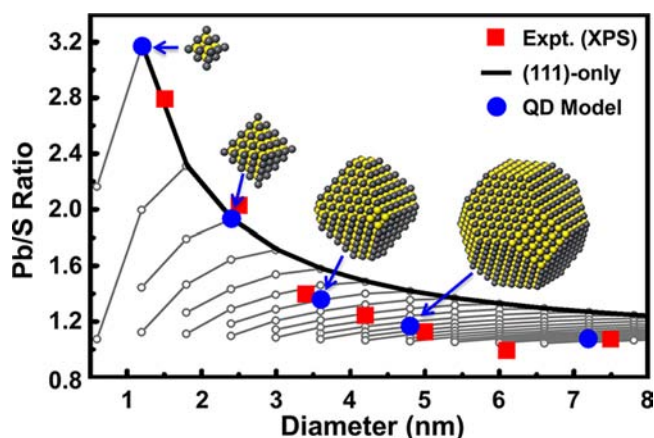


Figure 4. Pb/S ratio of octahedral and cuboctahedral PbS QD models as a function of diameter, compared with the XPS data. The (111)-only octahedral QDs show a deviation from experimental data at $D \approx 3$ nm. Proposed QD models are shown in the inset data, marked with blue circle.

Note that the proposed shape of QDs only represents the ensemble-averaged particle with the corresponding size because of the softness of PbS; thus the shape is less sharply defined than in “magic-sized clusters” of rather hard CdSe.¹⁶

In solution, the self-passivated semiconducting (100) surface may weakly interact with solvent molecules through the van der Waals-type interaction. On the other hand, the chemically passivated (111) surface will be mostly inert to other molecules. When cuboctahedral QDs are exposed to air, the unprotected (100) surface may undergo irreversible oxidation. This may be the origin of the air instability, blue shifts of the absorption edge, and p-type doping for large-size PbS QDs. In contrast, the octahedral QDs with full chemical passivation have no room for surface oxidation. This is why the ultrasmall QDs are so stable in ambient conditions. Careful replacement of oleate with a less hindered ligand during or after the synthesis will lead to atomically and microscopically surface-controlled air-stable PbS QDs.

In conclusion, we successfully synthesized air-stable ultrasmall PbS QDs. Detailed chemical analyses and theoretical simulations suggest that oleate-capped octahedral small-size QDs are very stable in air, while cuboctahedral large-size QDs truncated with the unpassivated (100) surface are rather unstable against surface oxidation. This microscopic understanding of QD surface chemistry, derived exclusively from ultrasmall PbS QDs, may pave the way to next-generation low-cost, high-efficiency QD photovoltaics.

■ ASSOCIATED CONTENT

📄 Supporting Information

Details of synthesis, characterization, and DFT simulation, and atomic coordinates of PbS QDs. This material is available free of charge via the Internet at <http://pubs.acs.org>.

■ AUTHOR INFORMATION

Corresponding Author

sjeong@kimm.re.kr; yong.hyun.kim@kaist.ac.kr

Author Contributions

[†]H.C. and J.-H.K. contributed equally.

Notes

The authors declare no competing financial interest.

■ ACKNOWLEDGMENTS

This work was supported by the Global Frontier R&D Program by the Center for Multiscale Energy Systems (2011-0031566), WCU program (R31-2008-000-10071-0), Industrial Core Grant (10035274), and NRF grant (2012-046191) funded by the Korea government (MEST).

■ REFERENCES

- (1) (a) Semonin, O. E.; Luther, J. M.; Choi, S.; Chen, H. Y.; Gao, J.; Nozik, A. J.; Beard, M. C. *Science* **2011**, *334*, 1530. (b) Sargent, E. H. *Nat. Photon.* **2009**, *3*, 325. (c) Luther, J. M.; Law, M.; Beard, M. C.; Song, Q.; Reese, M. O.; Ellingson, R. J.; Nozik, A. J. *Nano Lett.* **2008**, *8*, 3488.
- (2) Shockley, W.; Queisser, H. J. *J. Appl. Phys.* **1961**, *32*, 510.
- (3) Ip, A. H.; Thon, S. M.; Hoogland, S.; Voznyy, O.; Zhitomirsky, D.; Debnath, R.; Levina, L.; Rollny, L. R.; Carey, G. H.; Fischer, A.; Kemp, K. W.; Kramer, I. J.; Ning, Z.; Labelle, A. J.; Chou, K. W.; Amassian, A.; Sargent, E. H. *Nat. Nanotechnol.* **2012**, *7*, 577.
- (4) (a) Sykora, M.; Kopysov, A. Y.; McGuire, J. A.; Schulze, R. K.; Tretiak, O.; Pietryga, J. M.; Klimov, V. I. *ACS Nano* **2010**, *4*, 2021. (b) Moreels, L.; Fritzing, B.; Martins, J. C.; Hens, Z. *J. Am. Chem. Soc.* **2008**, *130*, 15081.
- (5) (a) Moreels, L.; Justo, Y.; De Geyter, B.; Haustraete, K.; Martins, J. C.; Hens, Z. *ACS Nano* **2011**, *5*, 2004. (b) Tang, J.; Brzozowski, L.; Barkhouse, D. A. R.; Wang, X.; Debnath, R.; Wolowicz, R.; Palmiano, E.; Levina, L.; Pattantyus-Abraham, A. G.; Jamakosmanovic, D.; Sargent, E. H. *ACS Nano* **2010**, *4*, 869.
- (6) (a) Hines, M. A.; Scholes, G. D. *Adv. Mater.* **2003**, *15*, 1844. (b) Lin, W.; Fritz, K.; Guerin, G.; Bardajee, G. R.; Hinds, S.; Sukhovatkin, V.; Sargent, E. H.; Scholes, G. D.; Winnik, M. A. *Langmuir* **2008**, *24*, 8215. (c) Abel, K. A.; Shan, J.; Boyer, J.; Harris, F.; Veggel, F. C. *J. M. Chem. Mater.* **2008**, *20*, 3794.
- (7) Baik, S. J.; Kim, K.; Lim, K. S.; Jung, S. M.; Park, Y. C.; Han, D. G.; Lim, S.; Yoo, S.; Jeong, S. *J. Phys. Chem. C* **2011**, *115*, 607.
- (8) Tang, J.; Liu, H.; Zhitomirsky, D.; Hoogland, S.; Wang, X.; Furukawa, M.; Levina, L.; Sargent, E. H. *Nano Lett.* **2012**, *12*, 4889.
- (9) (a) Hughes, B. K.; Ruddy, D. A.; Blakburn, J. L.; Smith, D. K.; Bergren, M. R.; Nozik, A. J.; Johnson, J. C.; Beard, M. C. *Nano Lett.* **2012**, *6*, 5498. (b) Chappell, H. E.; Hughes, B. K.; Beard, M. C.; Nozik, A. J.; Johnson, J. C. *J. Phys. Chem. Lett.* **2011**, *2*, 889.
- (10) (a) Bae, W. K.; Joo, J.; Padilha, L. A.; Won, J.; Lee, D. C.; Lin, Q.; Koh, W.; Luo, H.; Klimov, V. I.; Pietryga, J. M. *J. Am. Chem. Soc.* **2012**, *134*, 20160. (b) Luther, J. M.; Law, M.; Song, Q.; Perkins, C. L.; Beard, M. C.; Nozik, A. J. *ACS Nano* **2008**, *2*, 271. (c) Peterson, J. J.; Krauss, T. D. *Phys. Chem. Chem. Phys.* **2006**, *8*, 3851.
- (11) (a) Beard, M. C.; Midgett, A. G.; Law, M.; Semonin, O. E.; Ellingson, R. J.; Nozik, A. J. *Nano Lett.* **2009**, *9*, 836. (b) Cho, K. S.; Talapin, D. V.; Gaschler, W.; Murray, C. B. *J. Am. Chem. Soc.* **2005**, *127*, 7140. (c) Bealing, C. R.; Baumgardner, W. J.; Choi, J. J.; Hanrath, T.; Hennig, R. G. *ACS Nano* **2012**, *6*, 2118.
- (12) (a) Kim, Y.-H.; Heben, M. J.; Zhang, S. B. *Phys. Rev. Lett.* **2004**, *92*, 176102. (b) Feng, J.; Ding, S.-Y.; Tucker, M. P.; Himmel, M. E.; Kim, Y.-H.; Zhang, S. B.; Keyes, B. M.; Rumbles, G. *Appl. Phys. Lett.* **2005**, *86*, 033108. (c) Ko, S.-M.; Kim, J.-H.; Ko, Y.-H.; Chang, Y. H.; Kim, Y.-H.; Yoon, J.; Lee, J. Y.; Cho, Y.-H. *Cryst. Growth Des.* **2012**, *12*, 3838.
- (13) The definition of surface energy allows negative values for certain low-energy surfaces.
- (14) Ma, J.; Jia, Y.; Song, Y.; Liang, E.; Wu, L.; Wang, F.; Wang, X.; Hu, X. *Surf. Sci.* **2004**, *551*, 91.
- (15) Li, B.; Michaelides, A.; Scheffler, M. *Phys. Rev. B* **2007**, *76*, 075401.
- (16) Harrell, S. M.; McBride, J. R.; Rosenthal, S. J. *Chem. Mater.* **2013**, DOI: 10.1021/cm303318f.